

Inhomogeneous electronic states associated with charge-orbital order/disorder in $\text{BaV}_{10}\text{O}_{15}$ probed by photoemission spectromicroscopy

T. Yoshino,¹ K. Wakita,² E. Paris,³ A. Barinov,⁴ T. Kajita,⁵ T. Katsufuji,⁵ V. Kandyba,⁴ T. Sugimoto,⁶ T. Yokoya,² N. L. Saini,³ and T. Mizokawa¹

¹*Department of Applied Physics, Waseda University, Shinjuku, Tokyo 169-8555, Japan*

²*Research Institute for Interdisciplinary Science, Okayama University, Okayama 700-8530, Japan*

³*Department of Physics, University of Roma, La Sapienza, Piazzale Aldo Moro 2, 00185 Roma, Italy*

⁴*Sincrotrone Trieste S.C.p.A., Area Science Park, 34012 Basovizza, Trieste, Italy*

⁵*Department of Physics, Waseda University, Shinjuku, Tokyo 169-8555, Japan*

⁶*Department of Complexity Science and Engineering, University of Tokyo, Chiba 277-8561, Japan*

(Received 28 March 2017; revised manuscript received 10 August 2017; published 29 September 2017)

We have performed scanning photoemission spectromicroscopy of $\text{BaV}_{10}\text{O}_{15}$ across the metal-insulator transition at 123 K, which is accompanied by V $3d$ charge/orbital order and V trimerization. Nucleation of metallic domains is observed at the cleaved surface of $\text{BaV}_{10}\text{O}_{15}$ single crystals, similar to Cr-doped V_2O_3 in which electronic configurations of Cr^{3+} and V^{3+} are the same as those of V^{2+} and V^{3+} in $\text{BaV}_{10}\text{O}_{15}$. Typical domain size is $\sim 5\text{--}10\ \mu\text{m}$ at 150 K, just above the transition temperature. The metallic domains continuously grow up to 240 K, well above the transition temperature. The temperature evolution of the metallic phase in $\text{BaV}_{10}\text{O}_{15}$ is different from that of Cr-doped V_2O_3 , probably due to the charge degrees of freedom in $\text{BaV}_{10}\text{O}_{15}$.

DOI: [10.1103/PhysRevB.96.115161](https://doi.org/10.1103/PhysRevB.96.115161)

I. INTRODUCTION

Various transition-metal compounds such as VO_2 and V_2O_3 exhibit metal-insulator transitions (MITs) between metallic and insulating phases [1,2]. The MITs are usually accompanied by orderings of spin, charge, and/or orbital of transition-metal d electrons and by structural distortions of atomic arrangement. For example, the MIT in VO_2 is accompanied by the orbital ordering of V $3d\ t_{2g}$ and the V-V dimerization [3,4] while that in V_2O_3 is related to the V $3d\ t_{2g}$ orbital ordering and the complicated structural distortion [5–8]. Recently, Aetukuri *et al.* have demonstrated that the MIT in VO_2 can be controlled by manipulating the orbital occupancy with heterostructural engineering [4]. To develop future electronic devices by manipulating the MITs in VO_2 or other transition-metal oxides, it is highly important to observe domain structures of metallic and insulating phases in the bulk as well as at the surface/interface.

Scanning photoemission microscopy (SPEM) is a powerful technique for observing spatial modulation of band structure at surface. The metallic and insulating domain structure in colossal magnetoresistive Mn oxides [9] was revealed by imaging the density of states near the Fermi level (E_F) [10]. The metallic and insulating domain structure of Cr-doped V_2O_3 was revealed by SPEM [11,12]. Also, various inhomogeneous electronic states in transition-metal chalcogenides were studied by means of SPEM [13–15]. In contrast to the surface sensitive SPEM technique, infrared or x-ray absorption spectromicroscopy is rather bulk sensitive. The metallic and insulating domains in VO_2 were observed by means of infrared [16,17] and x-ray absorption spectromicroscopy [18]. It is known that metallic V oxides tend to exhibit insulating surface due to correlation-induced effect [19]. Therefore, it is very interesting to examine the relationship between the domain structures observed by the surface-sensitive and bulk-sensitive techniques in various V oxides.

Kajita *et al.* have established a new class of MIT in $\text{BaV}_{10}\text{O}_{15}$ which is accompanied by V $3d\ t_{2g}$ orbital ordering and V trimerization [20,21]. The optical absorption spectra of $\text{BaV}_{10}\text{O}_{15}$ exhibits a charge gap of $\sim 0.3\ \text{eV}$ in the insulating phase below 123 K [20]. In the metallic phase, the charge gap is destroyed and the Fermi edge is observed by hard x-ray photoemission spectroscopy (HAXPES) [22], although no Drude peak develops in the metallic phase above 123 K [20]. This behavior is similar to Cr-doped V_2O_3 , in which the paramagnetic metallic phase has a clear Fermi edge [23,24] and no Drude peak [11]. The absence of Drude peak is associated with the inhomogeneous electronic states observed by Lupi *et al.* using SPEM [11]. Although the SPEM is surface sensitive, the difference between the metallic and insulating regions can be detected clearly in Cr-doped V_2O_3 . Lupi *et al.* concluded that the SPEM image corresponds to space distribution of the topmost part of the metallic and insulating domains whose size is comparable to the probing depth of the optical spectroscopy [11]. Therefore, it is highly interesting to perform SPEM for $\text{BaV}_{10}\text{O}_{15}$ and to examine similarity and difference between Cr-doped V_2O_3 and $\text{BaV}_{10}\text{O}_{15}$. In addition to the MIT that can be applicable to electronic devices, $\text{BaV}_{10}\text{O}_{15}$ exhibits suppression of lattice thermal conductivity in the metallic phase due to the charge and orbital fluctuations [25]. The spatial distribution of charge-orbital ordered phases would play an important role in the scattering of acoustic phonons. In this sense, the SPEM study on $\text{BaV}_{10}\text{O}_{15}$ may provide useful information to understand the suppression of lattice thermal conductivity.

In this paper, we apply the SPEM technique to the surface of $\text{BaV}_{10}\text{O}_{15}$ with the unique MIT driven by V $3d$ charge and orbital orderings and V trimerization. The SPEM results on $\text{BaV}_{10}\text{O}_{15}$ indeed show inhomogeneous electronic states which can be associated with the MIT and the charge-orbital order/disorder.

II. EXPERIMENTAL

The SPEM results were obtained at the spectromicroscopy beamline, Elettra synchrotron facility, Italy [26]. Photons at 27 eV or 74 eV can be focused through a Schwarzschild objective to obtain a submicron size beam spot. In the present experiment, photon energy is set to 74 eV and the photoelectron excited from the near- E_F bands has k_z (momentum perpendicular to the surface) of $\sim 4.0 \text{ \AA}^{-1}$, approximately corresponding to $12\pi/c$ ($c \sim 9.39 \text{ \AA}$). The band structure calculation [27] predicts complicated Fermi surfaces that should be detected at this photon energy. For the present measurements, the total energy resolution was set to about 200 meV and the spatial resolution is $0.5 \mu\text{m}$. The measurements were performed under ultrahigh vacuum in the 10^{-10} Torr range. The sample was cleaved at 110 K and was studied by SPEM. Then it was heated to 150 K across the transition temperature of 123 K and spectral change across the transition was measured. The sample was heated further up to 210 K and SPEM data were taken at the elevated temperature well above the transition. Then it was cooled to 110 K to be measured again below the transition temperature. All the spectra were taken within 25 hours after the cleavage, and no signature of surface degradation (change of valence-band spectrum, depletion of near- E_F spectral weight, etc.) was detected during the measurement. A standard SPEM procedure was used to remove topographic features from the images presented [28].

III. RESULTS AND DISCUSSION

Figure 1(a) shows the valence-band photoemission spectra of $\text{BaV}_{10}\text{O}_{15}$ for 110 K, 150 K, and 210 K, which were obtained with $h\nu = 74 \text{ eV}$ and the angle-integrated mode. The V $3d$ and O $2p$ bands are ranging from E_F to -3 eV and from -3 to -9 eV , respectively. The relationship between the temperatures and the resistivity is illustrated in Fig. 1(b). Although the resistivity drops two orders of magnitude at the transition temperature at 123 K, the photoemission intensity at E_F does not change dramatically in going from 110 K to 150 K to 210 K. On the other hand, HAXPES results on $\text{BaV}_{10}\text{O}_{15}$ show a drastic spectral change in going from the insulating phase to the metallic phase, consistent with the resistivity jump [22]. This indicates that the surface region of $\text{BaV}_{10}\text{O}_{15}$ tends to be insulating even in the metallic phase. This tendency is very similar to V_2O_3 [23,24] and CaVO_3 [19], and the electronic correlation stabilizing the insulating state is enhanced in the vicinity of the surface. The valence-band spectra do not have the surface component of Ba $5p$, which is observed at the cleaved surface with Ba ions as reported in $\text{YBa}_2\text{Cu}_3\text{O}_7$ and $\text{PrBa}_2\text{Cu}_3\text{O}_7$ [29,30]. Therefore, the single crystals of $\text{BaV}_{10}\text{O}_{15}$ were cleaved between the V-O layers as shown in Fig. 1(c). Since the V-O bonds between the V-O layers play important roles for the MIT and are broken at the surface, the metallic phase would be suppressed further at the surface layer.

Figure 2(a) shows a photoemission intensity image of the entire crystal, which was taken at 110 K with $8.0 \mu\text{m}$ step just after the cleavage under the ultrahigh vacuum. The photoemission intensity image is obtained by integrating the photoemission spectrum of the valence band. The relatively

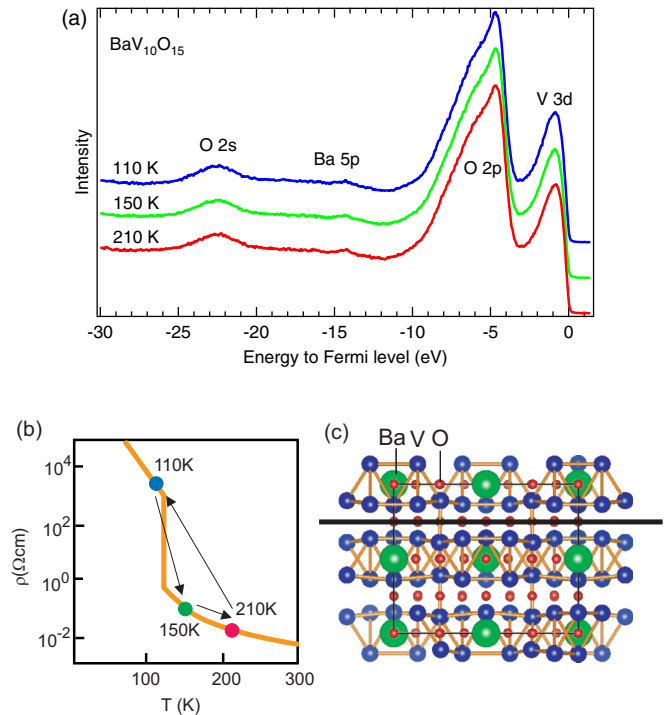


FIG. 1. (a) Photoemission spectra of the entire valence band of $\text{BaV}_{10}\text{O}_{15}$ taken at 110 K, 150 K, and 210 K. (b) Schematic drawing for resistivity of $\text{BaV}_{10}\text{O}_{15}$. The circles indicate the temperatures for photoemission measurements. The transition temperature is 123 K. (c) Crystal structure and cleavage plane of $\text{BaV}_{10}\text{O}_{15}$. The cleavage plane is indicated by the thick solid line.

flat region was selected, and a photoemission intensity image of the V $3d$ band was taken with $1.0 \mu\text{m}$ step, which is shown in Fig. 2(b). The photoemission intensity varies as a function of position due to height difference. It is expected that the low-binding energy part of the V $3d$ peak (from -0.5 eV to E_F) is sensitive to the MIT whereas the high-binding energy part of the V $3d$ peak [from -2.0 eV to -1.5 eV , see Fig. 1(a)] does not change across the MIT. Therefore, in order to remove the effect of height difference, the photoemission intensity image for spectral weight integrated from -0.5 eV to E_F is normalized to the spectral weight from -2.0 eV to -1.5 eV and is plotted with a different color scale in Fig. 2(c). The effect of height difference is indeed removed from the image.

Before showing temperature dependence, possible radiation effects should be discussed. After the photoemission intensity image in Fig. 2(c) was taken, the angle-integrated photoemission spectra with wide energy ranges were taken at several positions, keeping the focused beam at each position for several minutes. Then a new photoemission intensity image was taken, as shown in Fig. 2(d), where small spots with high intensity exist in the low-intensity background. The positions of the spots correspond to those for the angle-integrated photoemission measurements, indicating that the high intensity spots were induced by radiation effect. The photoemission spectra extracted from the image around the low intensity points (points A and D) and the high intensity points (points B and C) are compared in Fig. 2(e). The photoemission spectrum is integrated in the area of $3 \mu\text{m} \times 3 \mu\text{m}$, which is almost the

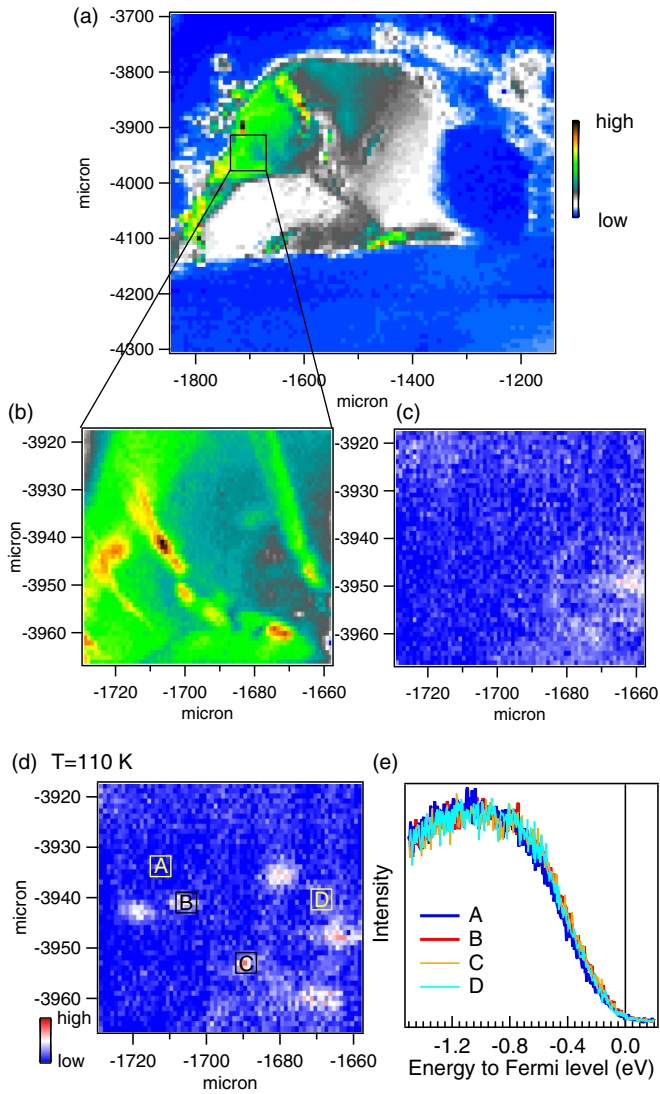


FIG. 2. (a) Photoemission intensity image of the entire crystal at 110 K. (b) Photoemission intensity image of the selected area indicated by the box in (a). (c) Normalized photoemission intensity image of the selected region at 110 K just after the cleavage. The spectral weight integrated from -0.5 eV to E_F is divided by that, integrated from -2.0 eV to -1.5 eV. (d) Normalized photoemission intensity image of the selected region at 110 K after taking spectra at several points. (e) $V 3d$ photoemission spectra extracted from (d) for the low intensity points, A and D, and the high intensity points, B and C.

size of the squares at the labels. At points B and C, the $V 3d$ peak is slightly shifted to E_F , compared to that at point A. However, the energy shift is much smaller than that due to the MIT, which will be discussed in the next paragraph. Therefore, one can safely discuss the effect of MIT from the temperature-induced spectral change that is much larger than the radiation-induced change.

Figure 3(a) shows the photoemission intensity image for 150 K (above the MIT temperature) with $0.5 \mu\text{m}$ step which is obtained by the same normalization procedure as the images in Figs. 2(c) and 2(d). Near- E_F intensity was enhanced in several regions of the image in going from 110 K to 150 K. The photoemission spectra of the high and low intensity points

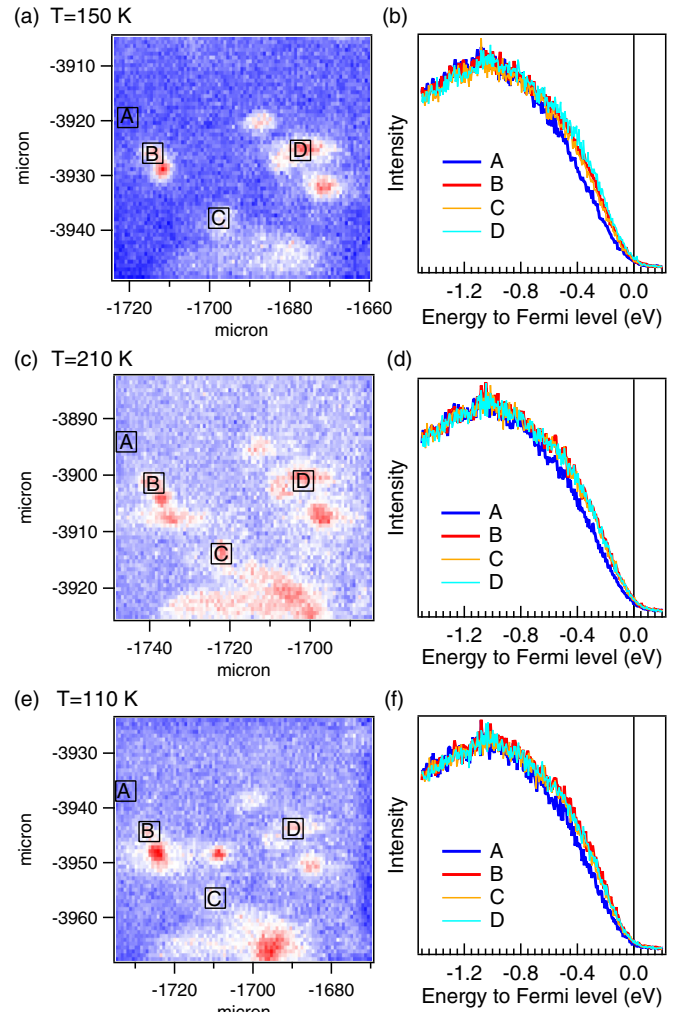


FIG. 3. (a) Normalized photoemission intensity image of the selected region taken at 150 K. (b) $V 3d$ photoemission spectra of the low intensity points and high intensity points in the intensity image at 150 K. (c) Normalized photoemission intensity image of the selected region taken at 210 K. (d) $V 3d$ photoemission spectra of the low intensity points and high intensity points in the intensity image at 210 K. (e) Normalized photoemission intensity image of the selected region taken at 110 K after the heating and cooling cycle. (f) $V 3d$ photoemission spectra of the low intensity points and high intensity points in the intensity image at 110 K after the heating and cooling cycle.

are compared in Fig. 3(b). At the high intensity point of D, the $V 3d$ band is shifted to E_F , compared to the low intensity point A. Near- E_F intensity of points B and C is intermediate between points A and D. Following the SPEM study on Cr-doped V_2O_3 [11], one can assume that the high intensity regions correspond to the topmost parts of the metallic domains in the bulk. The coexistence of the high and low intensity regions indicates that the bulk electronic state is inhomogeneous above the MIT temperature. In going from 150 K to 210 K, the high intensity regions were expanded further, as shown in Fig. 3(c). Figure 3(d) displays the $V 3d$ spectra for the high and low intensity points, which correspond to the metallic and insulating regions, respectively. At the high intensity points, the $V 3d$ band is shifted to E_F , compared to the low intensity

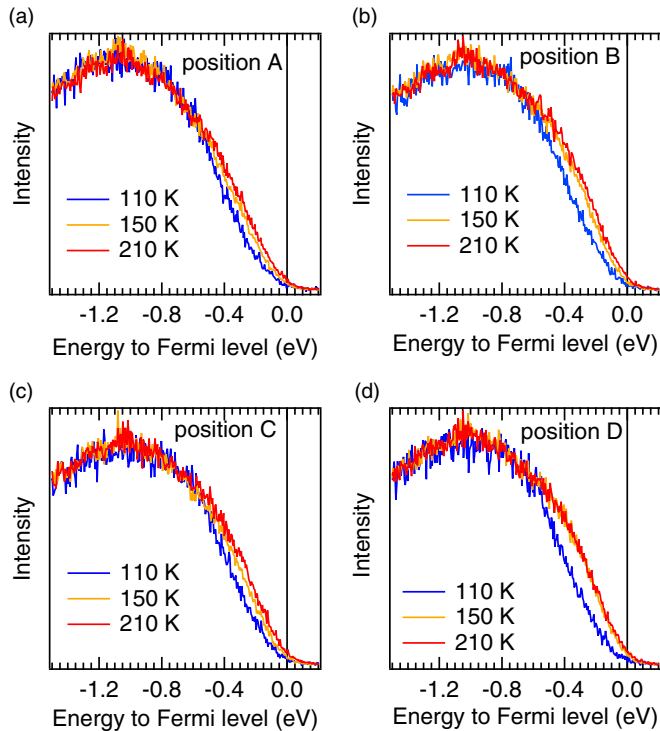


FIG. 4. (a)–(d) Temperature dependence of the V 3d spectral shape at points A–D.

point. When the crystal was cooled from 210 K to 110 K with reasonable cooling rate, the area of the high intensity region (or metallic region) was reduced. However, the metallic region still remains, exhibiting a kind of hysteresis, which should be related to the strong surface effect on the metallic state. As shown in Fig. 3(f), the spectral difference between the metallic and insulating regions is as large as that at 150 K. Once the lattice distortion for stabilizing the charge-orbital order is released above the MIT temperature, it may not be recovered and the metallic state may remain at the surface even below the MIT temperature.

The temperature dependence of the V 3d spectral shape at points A–D are summarized in Figs. 4(a)–4(d), respectively. Above the MIT temperature, point A belongs to the insulating region since the near- E_F intensity of point A is much smaller than that of point D. However, the near- E_F spectral weight at point A increases slightly in going from 110 K to 150 K. Therefore, the electronic structure of the insulating region at 150 K is different from that at 110 K. The spectral change across the MIT is very clear at point D, where the transition from the insulating state at 110 K to the metallic state at 150 K was realized.

Since the spectral weight at E_F of the metallic region is smaller than that observed in the HAXPES [22], the correlation effect is enhanced at the surface of $\text{BaV}_{10}\text{O}_{15}$, similar to the situation reported for V_2O_3 [24]. However, even in the bulk-sensitive HAXPES, the spectral weight at E_F is suppressed and a kind of pseudogap is formed in $\text{BaV}_{10}\text{O}_{15}$. On the other hand, no pseudogap was observed in the bulk-sensitive photoemission spectra on the metallic phase of Cr-doped and pure V_2O_3 [23,24]. This indicates that, above the MIT temperature, $\text{BaV}_{10}\text{O}_{15}$ is more inhomogeneous than

Cr-doped V_2O_3 . This speculation is indeed consistent with the present SPEM study.

In the vicinity of phase transitions, the system may fluctuate between two different ground states with nearly degenerate free energies. Here, one can speculate that nucleation of the metallic domains is governed by the defects created by the Cr doping or the disorder of $\text{V}^{2+}/\text{V}^{3+}$ charge order in case of Cr-doped V_2O_3 and $\text{BaV}_{10}\text{O}_{15}$, respectively. It is interesting to point out that the local electronic configurations of $\text{V}^{3+}(d^2)$ and $\text{Cr}^{3+}(d^3)$ in Cr-doped V_2O_3 are similar to those of $\text{V}^{3+}(d^2)$ and $\text{V}^{2+}(d^3)$ in $\text{BaV}_{10}\text{O}_{15}$. Also, the VO_6 octahedra share their edges and faces both in Cr-doped V_2O_3 and $\text{BaV}_{10}\text{O}_{15}$. In the d^3 configuration, the triply degenerate t_{2g} orbitals are occupied by three spin-up electrons satisfying Hund's rule. Therefore, it is reasonable to speculate that the species with d^3 tends to stabilize the insulating region when free energies of the metallic and insulating states are very close to each other in the vicinity of the transition. Namely, the Cr^{3+} and V^{2+} serve as a kind of anchor of the insulating region and suppress the nucleation of the metallic droplet even above the MIT temperature. Since the regions with radiation effect tend to be metallic above the MIT temperature, as shown in Fig. 3, some defects created by the radiation may promote nucleation of the metallic domains. The relative population of the metallic domains is rather small in $\text{BaV}_{10}\text{O}_{15}$. This would be related to the fact that resistivity gradually decreases with heating even above the MIT temperature of $\text{BaV}_{10}\text{O}_{15}$ [20] as illustrated in Fig. 1(b). The metallic domains grow rather slowly in $\text{BaV}_{10}\text{O}_{15}$ since the amount of V^{2+} is much larger than that of Cr^{3+} and the insulating domain with $\text{V}^{2+}/\text{V}^{3+}$ charge order is very robust with remaining lattice disorder even above the transition temperature.

IV. CONCLUSION

In conclusion, we have studied the inhomogeneous electronic state of $\text{BaV}_{10}\text{O}_{15}$ by means of SPEM. Nucleation of metallic regions is observed across the transition at the cleaved surface of $\text{BaV}_{10}\text{O}_{15}$ single crystals. The inhomogeneous electronic state of $\text{BaV}_{10}\text{O}_{15}$ is similar to Cr-doped V_2O_3 in which electronic configurations of Cr^{3+} and V^{3+} are the same as those of V^{2+} and V^{3+} in $\text{BaV}_{10}\text{O}_{15}$. The metallic regions correspond to the topmost part of the metallic domains in the bulk. Compared with the bulk electronic structure, the spectral weight at E_F is considerably suppressed even in the metallic region, indicating that the correlation effect is enhanced near the surface as commonly observed in various transition-metal oxides. The metallic regions continuously grow up to 210 K, well above the transition temperature. The continuous increase of the metallic regions with heating is consistent with the resistivity decrease with heating in the metallic phase.

ACKNOWLEDGMENTS

This paper was supported by CREST-JST (Grant No. JPMJCR15Q2) and Grant-in-Aids for Scientific Research from Japan Society for the Promotion of Science (JSPS) (Grants No. 26400321 and No. 16H04020). This research was partially supported by the Program for Advancing Strategic International Networks to Accelerate the Circulation of Talented Researchers from JSPS (Grant No. R2705).

- [1] M. Imada, Y. Tokura, and A. Fujimori, *Rev. Mod. Phys.* **70**, 1039 (1998).
- [2] D. I. Khomskii, *Transition Metal Compounds* (Cambridge University Press, 2014).
- [3] M. W. Haverkort, Z. Hu, A. Tanaka, W. Reichelt, S. V. Streltsov, M. A. Korotin, V. I. Anisimov, H. H. Hsieh, H.-J. Lin, C. T. Chen, D. I. Khomskii, and L. H. Tjeng, *Phys. Rev. Lett.* **95**, 196404 (2005).
- [4] N. B. Aetukuri, A. X. Gray, M. Drouard, M. Cossale, Li Gao, A. H. Reid, R. Kukreja, H. Ohldag, C. A. Jenkins, E. Arenholz, K. P. Roche, H. A. Dürr, M. G. Samant, and S. S. P. Parkin, *Nat. Phys.* **9**, 661 (2013).
- [5] C. Castellani, C. R. Natoli, and J. Ranninger, *Phys. Rev. B* **18**, 4945 (1978).
- [6] J.-H. Park, L. H. Tjeng, A. Tanaka, J. W. Allen, C. T. Chen, P. Metcalf, J. M. Honig, F. M. F. de Groot, and G. A. Sawatzky, *Phys. Rev. B* **61**, 11506 (2000).
- [7] A. Tanaka, *J. Phys. Soc. Jpn.* **71**, 1091 (2002).
- [8] F. Rodolakis, P. Hansmann, J.-P. Rueff, A. Toschi, M. W. Haverkort, G. Sangiovanni, A. Tanaka, T. Saha-Dasgupta, O. K. Andersen, K. Held, M. Sikora, I. Alliot, J.-P. Itié, F. Baudelet, P. Wzietek, P. Metcalf, and M. Marsi, *Phys. Rev. Lett.* **104**, 047401 (2010).
- [9] M. Uehara, S. Mori, C. H. Chen, and S.-W. Cheong, *Nature* **399**, 560 (1999).
- [10] D. D. Sarma, D. Topwal, U. Manju, S. R. Krishnakumar, M. Bertolo, S. La Rosa, G. Cautero, T. Y. Koo, P. A. Sharma, S.-W. Cheong, and A. Fujimori, *Phys. Rev. Lett.* **93**, 097202 (2004).
- [11] S. Lupi, L. Baldassarre, B. Mansart, A. Perucchi, A. Barinov, P. Dudin, E. Papalazarou, F. Rodolakis, J.-P. Rueff, J.-P. Itie, S. Ravy, D. Nicoletti, P. Postorino, P. Hansmann, N. Parragh, A. Toschi, T. Saha-Dasgupta, O. K. Andersen, G. Sangiovanni, K. Held, and M. Marsi, *Nat. Commun.* **1**, 105 (2010).
- [12] B. Mansart, A. Barinov, P. Dudin, L. Baldassarre, A. Perucchi, E. Papalazarou, P. Metcalf, S. Lupi, and M. Marsi, *Appl. Phys. Lett.* **100**, 014108 (2012).
- [13] M. Bendele, A. Barinov, B. Joseph, D. Innocenti, A. Iadecola, A. Bianconi, H. Takeya, Y. Mizuguchi, Y. Takano, T. Noji, T. Hatakeda, Y. Koike, M. Horio, A. Fujimori, D. Ootsuki, T. Mizokawa, and N. L. Saini, *Sci. Rep.* **4**, 5592 (2014).
- [14] T. Mizokawa, M. Bendele, A. Barinov, A. Iadecola, B. Joseph, T. Noji, Y. Koike, and N. L. Saini, *J. Phys. Soc. Jpn.* **85**, 033702 (2016).
- [15] D. Ootsuki, A. Barinov, S. Pyon, H. Ishii, K. Kudo, M. Nohara, E. Paris, M. Yablonskikh, V. Kandyba, A. Fujimori, T. Toriyama, T. Konishi, Y. Ohta, T. Mizokawa, N. L. Saini (unpublished).
- [16] M. M. Qazilbash, M. Brehm, Byung-Gyu Chae, P.-C. Ho, G. O. Andreev, Bong-Jun Kim, Sun Jin Yun, A. V. Balatsky, M. B. Maple, F. Keilmann, Hyun-Tak Kim, and D. N. Basov, *Science* **318**, 1750 (2007).
- [17] A. Frenzel, M. M. Qazilbash, M. Brehm, Byung-Gyu Chae, Bong-Jun Kim, Hyun-Tak Kim, A. V. Balatsky, F. Keilmann, and D. N. Basov, *Phys. Rev. B* **80**, 115115 (2009).
- [18] S. Kumar, J. P. Strachan, M. D. Pickett, A. Bratkovsky, Y. Nishi, and R. S. Williams, *Adv. Mater.* **26**, 7505 (2014).
- [19] K. Maiti, P. Mahadevan, and D. D. Sarma, *Phys. Rev. Lett.* **80**, 2885 (1998).
- [20] T. Kajita, T. Kanzaki, T. Suzuki, J. E. Kim, K. Kato, M. Takata, and T. Katsufuji, *Phys. Rev. B* **81**, 060405(R) (2010).
- [21] K. Takubo, T. Kanzaki, Y. Yamasaki, H. Nakao, Y. Murakami, T. Oguchi, and T. Katsufuji, *Phys. Rev. B* **86**, 085141 (2012).
- [22] T. Yoshino, M. Okawa, T. Kajita, S. Dash, R. Shimoyama, K. Takahashi, Y. Takahashi, R. Takayanagi, T. Saitoh, D. Ootsuki, T. Yoshida, E. Ikenaga, N. L. Saini, T. Katsufuji, and T. Mizokawa, *Phys. Rev. B* **95**, 075151 (2017).
- [23] S.-K. Mo, H.-D. Kim, J. D. Denlinger, J. W. Allen, J.-H. Park, A. Sekiyama, A. Yamasaki, S. Suga, Y. Saitoh, T. Muro, and P. Metcalf, *Phys. Rev. B* **74**, 165101 (2006).
- [24] F. Rodolakis, B. Mansart, E. Papalazarou, S. Gorovikov, P. Vilmercati, L. Petaccia, A. Goldoni, J. P. Rueff, S. Lupi, P. Metcalf, and M. Marsi, *Phys. Rev. Lett.* **102**, 066805 (2009).
- [25] T. Katsufuji, T. Okuda, R. Murata, T. Kanzaki, K. Takayama, and T. Kajita, *J. Phys. Soc. Jpn.* **85**, 013703 (2016).
- [26] P. Dudin, P. Lacovig, C. Fava, E. Nicolini, A. Bianco, G. Cautero, and A. Barinov, *J. Synchrotron Rad.* **17**, 445 (2010).
- [27] C. A. Bridges, J. E. Greedan, and H. Kleinke, *J. Solid State Chem.* **177**, 4516 (2004).
- [28] M. Marsi, L. Casalis, L. Gregoratti, S. Gunther, A. Kolmakov, J. Kovac, D. Lonza, and M. Kiskinova, *J. Electron Spectrosc. Relat. Phenom.* **84**, 73 (1997).
- [29] M. C. Schabel, C.-H. Park, A. Matsuura, Z.-X. Shen, D. A. Bonn, Ruixing Liang, and W. N. Hardy, *Phys. Rev. B* **55**, 2796 (1997).
- [30] T. Mizokawa, C. Kim, Z.-X. Shen, A. Ino, A. Fujimori, M. Goto, H. Eisaki, S. Uchida, M. Tagami, K. Yoshida, A. I. Rykov, Y. Siohara, K. Tomimoto, and S. Tajima, *Phys. Rev. B* **60**, 12335 (1999).